

# Analyses of Distributions of Different Impurities for Growth of Polysilicon Ingots in Directional Solidification System

Guoxiang Peng,<sup>1</sup> Min-Chieh Kang,<sup>2</sup> Chao-Ming Hsu,<sup>2,\*</sup> and Cheng-Fu Yang<sup>3,4\*\*</sup>

<sup>1</sup>School of Ocean Information Engineering, Jimei University, Xiamen, Fujian 361021, China

<sup>2</sup>Department of Mechanical Engineering, National Kaohsiung University of Science and Technology, Kaohsiung 807, Taiwan

<sup>3</sup>Department of Chemical and Materials Engineering, National University of Kaohsiung, Kaohsiung 811, Taiwan

<sup>4</sup>Department of Aeronautical Engineering, Chaoyang University of Technology, Taichung 413, Taiwan

(Received April 18, 2023; accepted June 29, 2023)

**Keywords:** Ansys Fluent, simulation, finite volume method, argon gas inlet flow channel

This paper primarily focuses on simulating the variation of different impurity concentrations during the growth of polysilicon ingots. The simulation prototype employed was a directional solidification crystal growth furnace, and the governing equations of the Ansys Fluent module's finite analysis software were utilized. The simulation models used in this study included the energy, flow field, phase change (solidification and melting), heat transfer, species transport, and finite volume models. The simulation outcomes were validated using process data from Eversol Technology Co., Ltd., Taiwan. This paper explores the concentration distributions of impurities, such as oxygen and carbon elements, in argon and molten silicon during the general crystal growth process. The simulation results indicate that during the initial 5 h of polysilicon growth, the input of a large amount of argon can be used to eliminate impurities. Moreover, the results suggest that reducing the argon flow rate at the inlet at about 30 h, in the late stage of polysilicon growth, can lead to a more uniform temperature distribution in the polysilicon ingot. To enhance the quality of the grown polysilicon ingot, the impurities were concentrated in the upper part of the ingot. Additionally, the volume of air extracted at the gas outlet was increased over time to decrease the concentrations of impurities in the gas phase in the growth furnace.

## 1. Introduction

A directional solidification system grows polysilicon ingots through directional solidification. This principle involves the growth of the ingot in a single crystallization direction, with cooling occurring in the opposite direction to the grain growth. The aim is to achieve primarily axial heat transfer within the crucible where the polysilicon is grown, resulting in a straight solid–liquid interface. The shape of the solid–liquid interface in the polysilicon ingot is intricate, and measuring the physical properties of molten silicon in the growth crucible is costly. Alternatively, the physical properties of the furnace body, including the temperature distribution in the growth

---

\*Corresponding author: e-mail: [jammy@nkust.edu.tw](mailto:jammy@nkust.edu.tw)

\*\*Corresponding author: e-mail: [cfyang@nuk.edu.tw](mailto:cfyang@nuk.edu.tw)

<https://doi.org/10.18494/SAM4460>

crucible, the growth rate of the polysilicon ingot, and the concentration and distribution of impurities in the ingot, can be estimated through computer numerical simulation methods.<sup>(1–4)</sup> Moreover, simulation methods can assess various growth parameters such as the heater power, the argon inflow and outflow, and the height of the insulating cage. These methods can also predict the solid–liquid interface contour by numerically simulating the curvature in the growth crucible for different thermal field designs. Thus, numerical simulation methods are an ideal tool for investigating impurity transfer during polysilicon growth, facilitating the understanding of polysilicon ingot manufacturing processes for solar cells.

In the growth of high-quality polysilicon ingots, it is essential to avoid impurities in the raw materials and contamination during crystal growth, which could adversely affect the conversion efficiency of solar cells. Silicon raw materials commonly contain impurities such as oxygen, carbon, boron, phosphorus, and metals. Geerligs *et al.*,<sup>(5)</sup> Buonassisi *et al.*,<sup>(6)</sup> and Binetti *et al.*<sup>(7)</sup> pointed out that the lower the impurity concentration in the polysilicon ingot, the higher the conversion efficiency of solar cells.

During polysilicon growth, the silicon element in molten silicon chemically reacts with various impurities, resulting in the formation of compounds such as silicon oxide (SiO), silicon carbide (SiC), and silicon nitride (Si<sub>3</sub>N<sub>4</sub>). Oxygen impurity can originate from silicon raw materials, quartz crucibles, and residual oxygen in argon. Oxygen impurity can reduce the light conversion efficiency of solar cells, leading to lower product yields. Kvande *et al.* and Liu *et al.* discovered that the distribution of oxygen concentrations in the vertical direction is inversely proportional to the cooling rate.<sup>(8,9)</sup> Raabe *et al.* observed that impurities on the surface of graphite components can chemically react with oxygen in argon, with the resulting products entering the molten silicon.<sup>(10)</sup> Small amounts of oxygen and SiC precipitates have also been detected in silicon ingots. As molten silicon solidifies into solid silicon, impurities in the molten silicon can cause bottom sediments to accumulate on the top of the silicon ingot due to the segregation effect.<sup>(11,12)</sup> As a result of this effect, SiO can adsorb metal impurities and accumulate on the top of the silicon ingot. A high concentration of impurities can reduce the conversion efficiency of solar cells; thus, the impurity concentration should be minimized.<sup>(13)</sup>

This paper mainly focuses on the simulation-based analysis of impurity diffusion and segregation during the solidification and growth of polysilicon ingots. Although various furnaces for growing polysilicon ingots that are based on the principle of directional solidification have been manufactured, we use data generated from the GT-DSS450 model, a polysilicon ingot growth furnace manufactured by GT-Solar Company of the United States, to conduct numerical simulation-based analysis. The simulation utilized Fluent, a software package within the Ansys module, which includes energy, flow field, phase change (solidification and melting), heat transfer, species transport, and finite volume models. The internal structures of the polysilicon growth furnace were defined, including the argon gas inlet/outlet, crystal growth furnace wall, insulating cage, graphite shield, quartz crucible, heat sink, and heater. This article mainly focuses on simulating and analyzing impurity diffusion and segregation during the solidification and growth process of polycrystalline silicon ingots.

## 2. Simulation Process and Use of Parameters

To reduce the computational requirements in modeling the growth of polysilicon crystals, a local model was developed that focuses on the molten silicon, crucible, and crystal silicon as the primary objects for simulation. This model was created to optimize the overall calculations. Vizman *et al.* utilized STHAMAS 3D software to conduct a local model simulation for the 3D-layer flow of molten polysilicon.<sup>(14)</sup> Delannoy *et al.* employed dynamic grids to calculate the 3D outward appearance of silicon growth in a furnace and utilized the temperature gradient to determine the growth rate of the silicon ingot.<sup>(15)</sup> Dropka *et al.* observed that the distributions of streamlines had comparable disparities across various turbulence modes, while the magnitude of the direction vector exhibited substantial differences.<sup>(16)</sup> Thus, in this study, the transient mode was used to simulate the internal state of the polysilicon growth furnace. It was assumed that the furnace's temperature was optimized by allowing convection with the surrounding environment through the use of raised insulating cages on both sides. The simulation time for the crystal growth process was approximately 40 h, and the simulation parameters, including the argon flow rate, were based on the actual growth process. In this regard, the temperature of each segment in the furnace was set at 1685 K, with the temperature inside the molten silicon assumed to be 1750 K. Additionally, the furnace pressure was maintained at 200 millibars (mbar). Due to the presence of a water cooling system on the polysilicon growth furnace wall, the temperature was assumed to be 1000 K.

During the simulation of impurity concentrations, the primary factors of interest were the argon region, the gas–liquid interface, the quartz crucible wall, and the solid–liquid interface of the polysilicon crystal growth furnace. The impurity concentration distributions were analyzed in four directions, and the mechanisms of the diffusion and segregation effects among impurities within the polysilicon ingot were examined. During the growth process, argon gas was introduced above the furnace body to enhance the yield of the polysilicon ingot. Such protection of the surface of the molten silicon with an inert gas prevented chemical reactions with impurities present in the furnace. Moreover, the argon gas flow field helps eliminate any volatile impurities present in the molten silicon. According to information provided by Eversol Technology Co. Ltd., industrial-grade argon with a purity of 5N (99.999%) contains an oxygen concentration of below 2 parts per million (ppm), while argon with a purity of 99.9995% has a carbon monoxide (CO) concentration of less than 1 ppm. The impurity concentrations for argon with different purities were obtained from Rising Gas and are presented in Table 1.<sup>(17)</sup> Oxygen

Table 1  
Impurity concentrations for different purities of argon for industrial use.<sup>(17)</sup>

Argon purity (%)	99.999	99.9995	99.9997	99.9999
N <sub>2</sub> (ppm)	<5	<5	<3	<0.4
O <sub>2</sub> (ppm)	<2	<0.5	<0.5	<0.2
H <sub>2</sub> (ppm)	<1	—	—	—
CO (ppm)	—	<1	<0.5	<0.1
CO <sub>2</sub> (ppm)	—	<1	<0.5	<0.1
Moisture (ppm)	<4	<0.5	<0.5	<0.2

reacts with carbon on the surface of graphite components inside the furnace, forming CO in the argon gas region above the silicon melt. The CO is then carried into the silicon melt by the argon gas. Thus, the purity of argon gas affects the concentration of impurities in the silicon ingot manufacturing process, and these parameters in Table 1 can be used for simulation.

The primary objective of this study was to perform full-structure simulation analyses of the growth process of polysilicon in a directional solidification crystal growth furnace. To achieve this, a 2D asymmetric model was developed using AutoCAD software. The crystal growth furnace was equipped with two temperature sensors, namely thermocouple 1 (TC1) and thermocouple 2 (TC2). TC1 was placed to monitor the temperature of the heater, whereas TC2 was placed to monitor the temperature at the bottom of the graphite shield. The positions of TC1 and TC2 are depicted in Fig. 1. A water cooling system was installed inside the furnace wall to maintain its outside temperature at room temperature. The analyses employed transient state simulation to model the growth process of the polysilicon ingot, and the obtained simulation results were analyzed and discussed to determine the changes in the impurity diffusion distributions within the crystal growth furnace. The duration of the polysilicon ingot growth process for this study was 40 h. The internal boundaries of the crystal growth furnace were categorized into three regions: the insulating cage movement area on both sides, the gas–liquid interface between the argon and molten silicon, and the impurity concentration boundary in the molten silicon. These boundaries are illustrated in Fig. 1. The pressure within the crystal growth furnace was maintained at 200 mbar, and the initial temperatures of each element within the furnace and the molten silicon were set at 1685 and 1750 K, respectively.

The numerical analyses employed the actual process data from point TC1 to control the heater function. A curve-fitting method was used to derive five-segment functions, which were then utilized to produce time–temperature variations originating from the heater variations through the heater. During the early stages of polysilicon growth, the temperature of TC1 was set to 1758 K, then it was decreased to 1689 K during the later stages. The five-segment functions were as follows, where  $y$  is the temperature and  $x$  is the time:

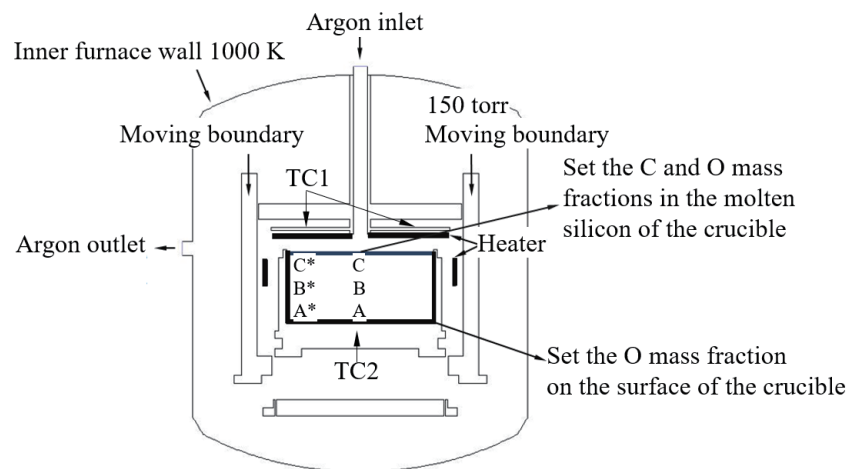


Fig. 1. Schematic diagram of the boundaries of the directional solidification crystal growth furnace.

$$y_1 = 1486.9 - 70.3x \quad (1)$$

$$y_2 = 1427.3 + 0.81x \quad (2)$$

$$y_3 = 1438.6 - 1.36x + 0.04x^2 - 4.95 \times 10^{-4}x^3 \quad (3)$$

$$y_4 = 1460.7 - 1.22 \times 10^{-4}x \quad (4)$$

$$y_5 = 1441.6 - 0.67x \quad (5)$$

The software, research items, and operation steps can be broadly divided into four stages: pre-processing, boundary condition setting, numerical analysis, and post-processing. During the pre-processing, a 2D geometric model was built using AutoCAD. This model was then repaired and component names were assigned using Ansys Design Modeler. Finally, Ansys Mesh was used to create a mesh. During the boundary condition setting, the flow rate of argon gas at the inlet and outlet, the temperature and pressure of the furnace wall, the initial temperature field of molten silicon, and the mass fraction of impurities were established. Certain material properties were temperature-dependent functions and required the use of Visual Studio functions to load Fluent user-defined functions via the library mount mode. During the numerical analysis, the calculations were performed using Fluent, and the finite volume method was used to solve for the material parameters, velocity field, temperature field, and impurity concentration. The related mathematical models were corrected using the SIMPLEC function library in the coupled mode. For post-processing, the post-processing function of Fluent was used to export the calculation results, and the data from Ansys Workbench was utilized for processing.

### 3. Simulation Results and Discussion

The results of the numerical analyses were used to discuss the temperature fields and concentration gradient distributions of non-metallic impurities (oxygen and carbon) in the gas, liquid, and solid phases in the crystal growth furnace. The impurities in the gas phase mostly originated from argon, with a small proportion originating from various furnace components. During the operation of the furnace, the oxygen impurity present in the argon gas reacts with the graphite components due to the high-temperature environment. However, since only a small amount of oxygen molecules remains in the argon gas, the main product generated by this reaction is CO. This CO gas flows into the molten silicon in the direction of the airflow, leading to the formation of SiC and SiO impurities in the final polysilicon ingot. The numerical analyses provided insight into the mechanism by which the impurity concentrations change in the gas phase and can serve as a reference for future optimization of the polysilicon growth process. Initially, the temperature field distributions in the furnace were simulated. Figure 2 illustrates the overall temperature field distributions after 5, 10, 15, 20, 25, 30, 35, and 40 h of growth of the polysilicon ingot. The results shown in Fig. 2 also suggest that reducing the argon flow rate at the inlet at about 30 h, in the late stage of polysilicon growth, can lead to a more uniform

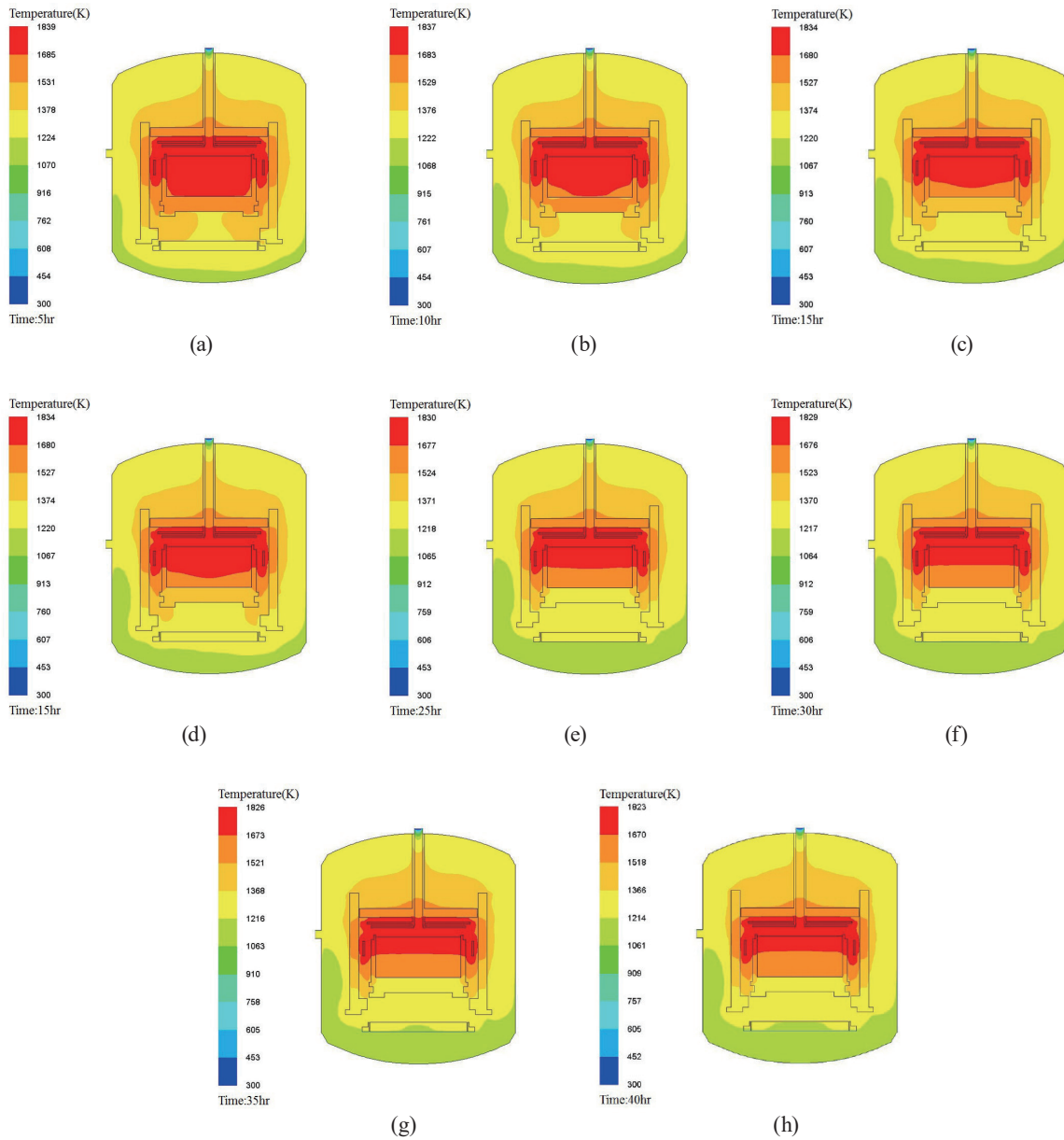


Fig. 2. (Color online) Distributions of temperature in the polysilicon growth furnace after (a) 5, (b) 10, (c) 15, (d) 20, (e) 25, (f) 30, (g) 35, and (h) 40 h.

temperature distribution in the polysilicon ingot. The simulation results demonstrate that the bottom of the polysilicon ingot gradually cools, and the heat energy in the furnace is transferred out through the bottom gap as the insulating cage moves upward. Moreover, the temperature gradient in the molten silicon exhibits a cooling trend in the initial stage of the polysilicon growth, and the cooling rate in the central area becomes greater than that at the crucible edge as time elapses.

Figure 3 displays the distribution of the CO concentration in the gas phase every 5 h during the growth of the polysilicon ingot. Figures 3(a)–3(d) indicate that the CO concentration in the

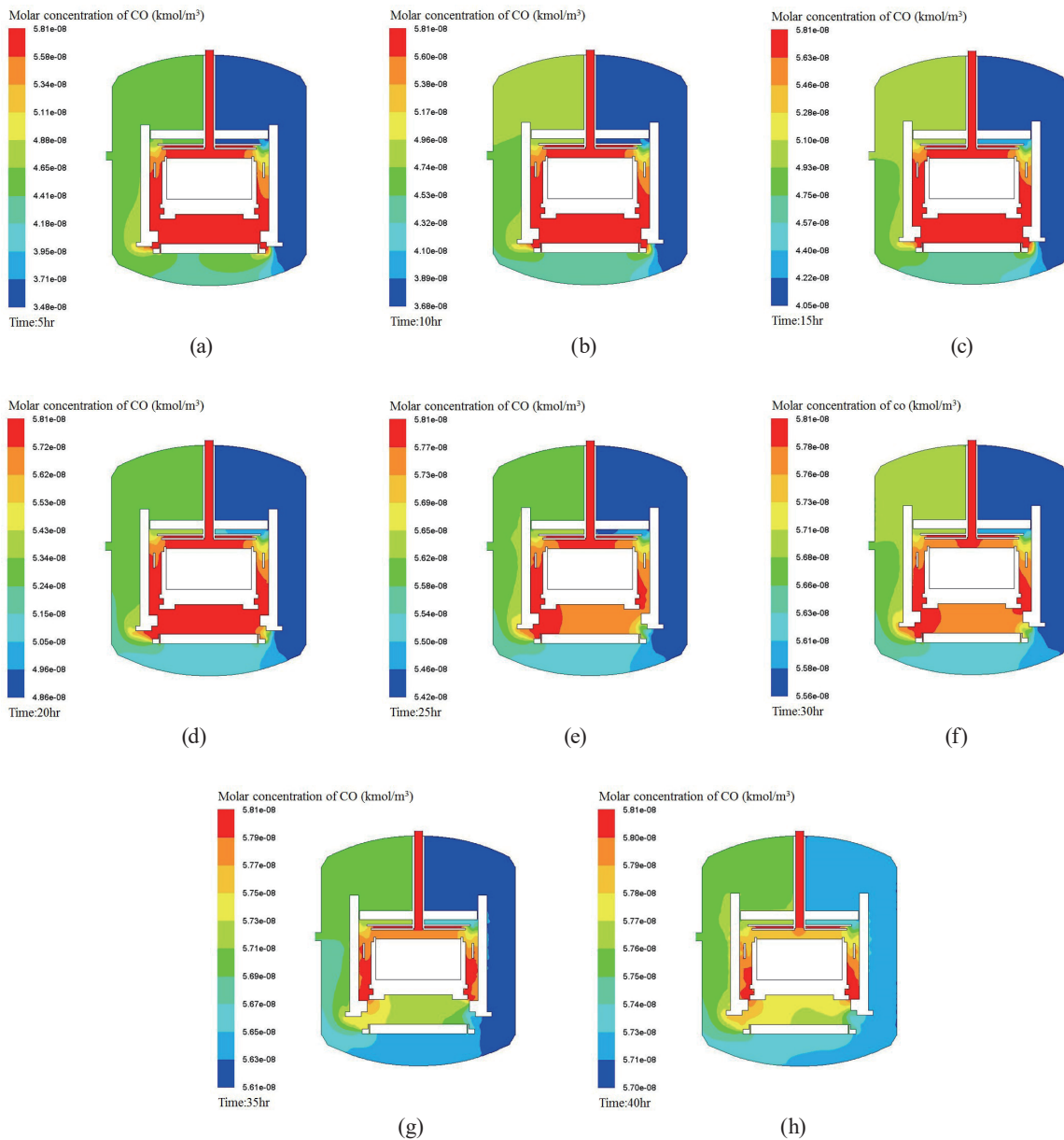


Fig. 3. (Color online) Distributions of CO concentration in the gas phase after (a) 5, (b) 10, (c) 15, (d) 20, (e) 25, (f) 30, (g) 35, and (h) 40 h.

furnace is initially unevenly distributed, with the CO concentrated in the central region of the furnace. This uneven distribution is attributed to the presence of an air outlet on the left side, which continuously removes CO from the furnace. This results in a maximum difference of approximately  $1.54 \times 10^{-8}$  kmol/m<sup>3</sup> between the oxygen concentrations on the left and right sides. Additionally, the carbon impurity present in the graphite element reacts with oxygen on the surface of the molten silicon during the process, producing CO. Figures 3(a)–3(h) demonstrate that the maximum CO concentration above the molten silicon is  $5.81 \times 10^{-8}$  kmol/m<sup>3</sup>. This indicates that excess CO may dissolve in the molten silicon, potentially generating carbon

and oxygen impurities within the polysilicon ingot. The CO concentration is higher on the left side of the furnace due to the influence of the argon flow drawing. According to the data provided by Eversol Technology Co. Ltd., the amount of argon in the polysilicon growth furnace decreases slightly over time during the actual process. Figure 3(h) illustrates that the CO concentration in the furnace gradually saturates after 40 h. Consequently, to avoid excessive CO entering the molten silicon, it is necessary to increase the pumping capacity of the argon outlet.

Figure 4 illustrates the distribution of the oxygen concentration in the gas phase during the growth of the polysilicon ingot from 5 to 40 h. Analysis of Figs. 4(a)–4(h) reveals that the oxygen concentration in the furnace is initially non-uniformly distributed, with oxygen concentrated in

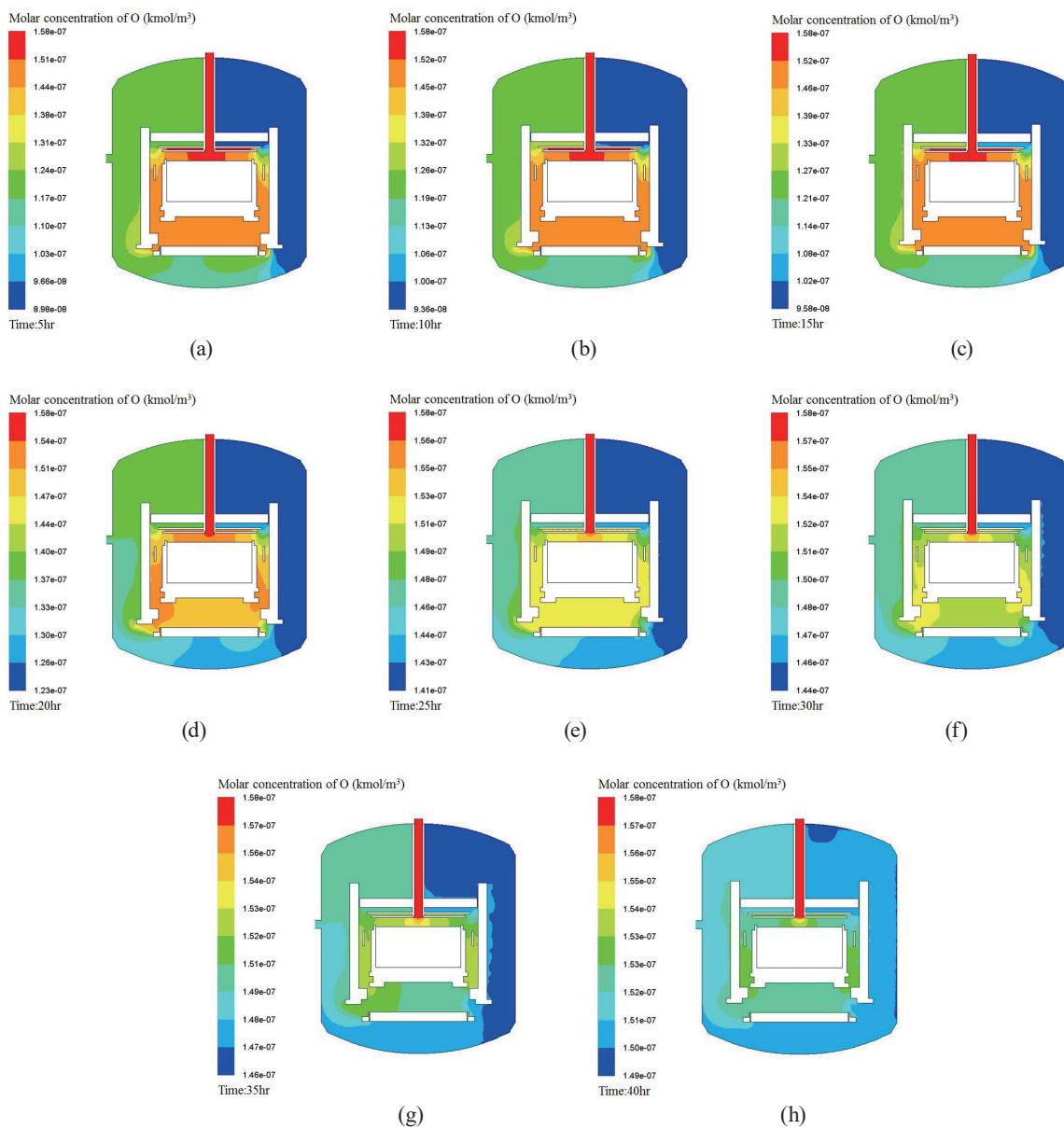


Fig. 4. (Color online) Distributions of oxygen concentration in the gas phase after (a) 5, (b) 10, (c) 15, (d) 20, (e) 25, (f) 30, (g) 35, and (h) 40 h.

the argon tube and the vicinity of the gas inlet, as demonstrated in Fig. 4(b). In the early stages of the polysilicon growth process, the oxygen concentration on the right side of the furnace is higher than that on the left side. This is because the gas outlet on the left side continuously extracts the gas in the furnace, which causes the oxygen concentration to move in the direction of the argon flow field. The oxygen concentration distributions obtained from the analysis are presented in Figs. 4(a)–4(h). The maximum difference between the left and right oxygen concentrations is approximately  $3.32 \times 10^{-8}$  K mol/m<sup>3</sup>. The simulation results indicate that the oxygen concentration in the central region gradually diffuses to the surrounding area as the polysilicon ingot progresses through the growth stage. This is primarily attributed to the gradual upward movement of the insulating cage inside the furnace and the consequent increase in the bottom gap. As a result, the gas in the furnace diffuses outward through this gap, leading to the outcomes presented in Figs. 4(a)–4(g). Furthermore, during the polysilicon growth, oxygen on the graphite element reacts with carbon to produce CO. If this CO impurity accumulates above the molten silicon, it may dissolve into the molten silicon. Consequently, the presence of this impurity in the polysilicon ingot leads to contamination, resulting in reduced conversion efficiency and solar cells with a lower yield. Therefore, it is crucial to reduce the concentrations of carbon and oxygen impurities in the polysilicon growth furnace. Finally, when the insulating cage descends to the bottom, the gas in the furnace attains an equilibrium state, and the highest concentration of oxygen is observed in the air inlet pipe, as illustrated in Fig. 4(h).

The majority of the oxygen impurity arises from the wall of the quartz crucible and the silicon raw material, with a minority attributed to the argon, which is doped into the molten silicon during the polysilicon growth. The oxygen impurity leads to the formation of compounds such as SiO and SiO<sub>2</sub>, reducing the conversion efficiency of solar cells. Hence, numerical analysis can aid in comprehending the process underlying the variation in the oxygen impurity concentration in the solid phase, serving as a reference for optimizing the polysilicon growth process in the future. The simulation results of the oxygen concentration were analyzed, and the distributions of the oxygen impurity concentration in the solid–liquid phase during the polysilicon growth process from 5 to 40 h are presented in Fig. 5. The results reveal that a large amount of oxygen impurity is generated following the dissolution of the quartz crucible wall, resulting in a higher oxygen concentration at the periphery of the quartz crucible than in its central region. Figures 5(a)–5(g) reveal that the oxygen concentration in the central area gradually moves upwards due to the segregation effect. As depicted in Fig. 5(h), the oxygen impurity eventually concentrates at the top of the polysilicon ingot. Figure 6 displays the fluctuation in the oxygen impurity concentration at different points in the central region during each time period. The concentrations at points A–C in the central area after 5 h are  $2.54 \times 10^{-7}$ ,  $3.31 \times 10^{-7}$ , and  $4.72 \times 10^{-7}$  kmol/m<sup>3</sup>, and those after 20 h, midway through the process, are  $2.74 \times 10^{-7}$ ,  $3.57 \times 10^{-7}$ , and  $5.04 \times 10^{-7}$  kmol/m<sup>3</sup>, respectively.

According to the simulation results, the oxygen concentrations at points A–C progressively increase with time due to the segregation effect of the oxygen impurity, leading to the partial retention of oxygen in the crystal polysilicon ingot. Eventually, the oxygen concentrations at points A–C reach  $2.75 \times 10^{-7}$ ,  $3.59 \times 10^{-7}$ , and  $5.06 \times 10^{-7}$  kmol/m<sup>3</sup>, respectively. As also shown in Fig. 6, the oxygen concentration gradually decreases as the depth of the polysilicon ingot

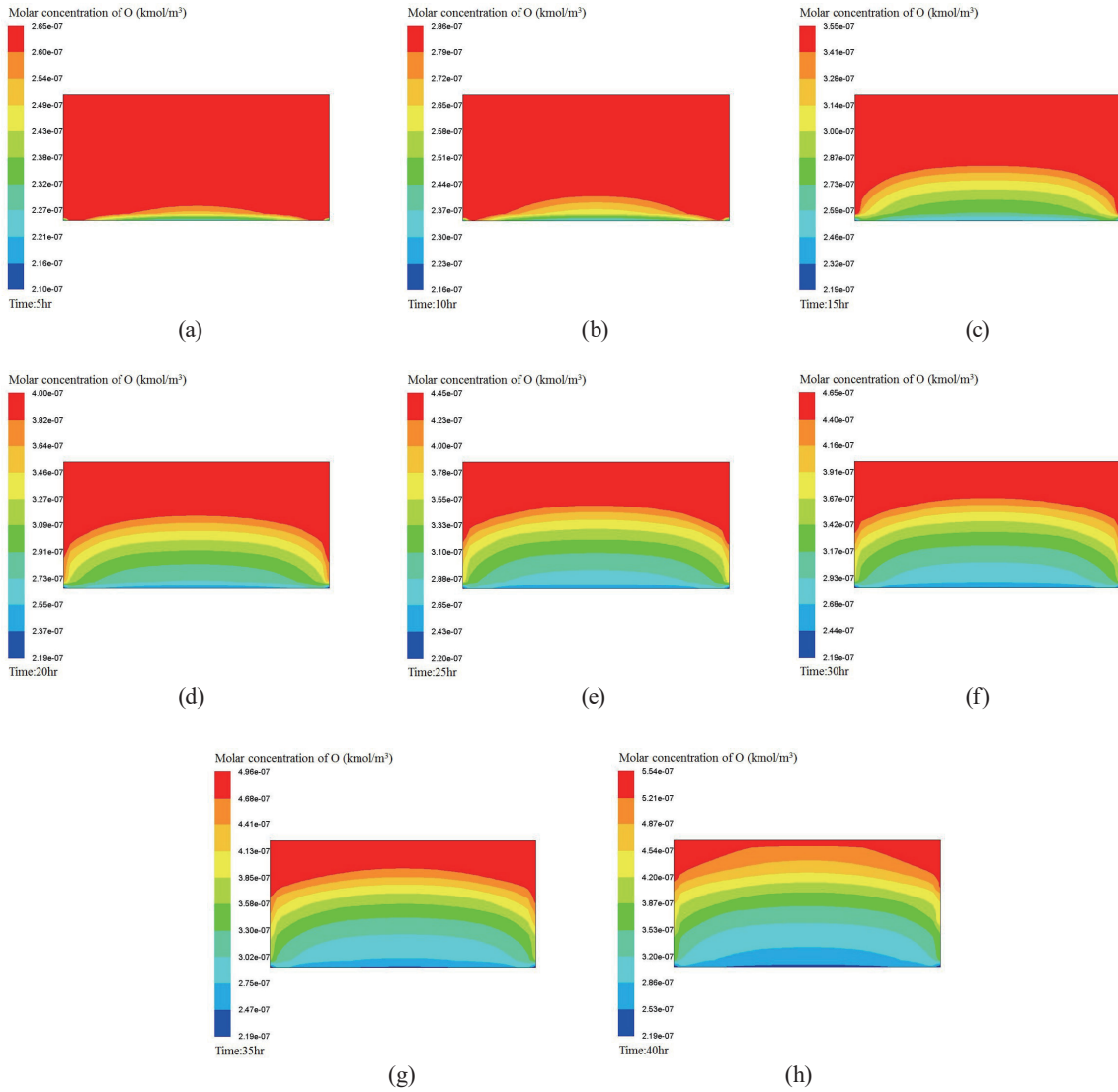


Fig. 5. (Color online) Distributions of oxygen concentration in the solid–liquid phase after (a) 5, (b) 10, (c) 15, (d) 20, (e) 25, (f) 30, (g) 35, and (h) 40 h.

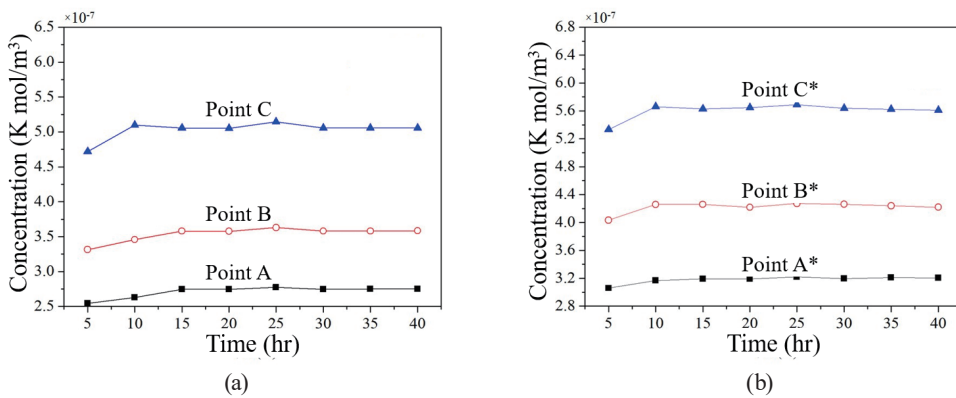


Fig. 6. (Color online) Distributions of oxygen concentration in (a) central area and (b) quartz crucible area.

increases, suggesting that the oxygen tends to diffuse into the ingot as the growth progresses. This figure illustrates that the oxygen impurity concentration in the crucible area is higher than that in the central area due to the generation of a large amount of oxygen impurity after the heating and dissolution of the quartz crucible. Points A\*, B\*, and C\* are within the crucible area. The oxygen impurity concentrations at points A\*, B\*, and C\* increase from  $3.06 \times 10^{-7}$ ,  $4.03 \times 10^{-7}$ , and  $5.33 \times 10^{-7}$  kmol/m<sup>3</sup> at 5 h to  $3.21 \times 10^{-7}$ ,  $4.22 \times 10^{-7}$ , and  $5.61 \times 10^{-7}$  kmol/m<sup>3</sup> at 40 h, respectively. These results indicate that the oxygen impurity tends to diffuse into the polysilicon ingot. The results also demonstrate the utility of numerical analysis in comprehending the mechanism behind the change in the oxygen impurity concentration in the solid phase during polysilicon growth. Going forward, it is imperative to take into account strategies for minimizing oxygen impurity diffusion into the crystal polysilicon ingot during growth.

The majority of the carbon impurity in the polysilicon growth furnace originates from the graphite components, while some originates from the silicon raw material. At high temperatures, the oxygen impurity in the argon gas reacts with the graphite components, producing CO. This gas enters the molten silicon via the airflow and transforms into the impurity SiC within the polysilicon ingot, even if the oxygen atom concentration is low. Figure 7 depicts the distributions of the carbon impurity concentration in the solid and liquid phases during the polysilicon growth process from 5 to 40 h. The carbon impurity is subject to both diffusion and segregation effects in the molten silicon. As a result, the carbon concentration diffuses along the temperature gradient curve and subsequently accumulates at the top of the polysilicon ingot through the segregation effect. Figures 7(a)–7(f) indicate that the carbon concentration in the central region is higher than that at the crucible edge and, due to the segregation effect, most of the carbon impurity slowly moves upward. As shown in Fig. 7(h), the carbon impurity eventually concentrates at the top of the polysilicon ingot. During the solidification of the ingot, the segregation coefficient of the carbon impurity is 0.07, resulting in a higher concentration of carbon impurity in the molten silicon than in the polysilicon crystal.

Figure 8(a) illustrates the variation of the carbon impurity concentration in the central area as a function of growth time and position. At 5 h, the concentrations at points A–C are  $2.41 \times 10^{-7}$ ,  $2.43 \times 10^{-7}$ , and  $2.48 \times 10^{-7}$  kmol/m<sup>3</sup>, respectively, with little variation among the positions. At 20 h, the concentrations at points A–C are  $2.38 \times 10^{-7}$ ,  $2.42 \times 10^{-7}$ , and  $2.51 \times 10^{-7}$  kmol/m<sup>3</sup>, respectively. The carbon impurity concentration at points A and B decreases with time, whereas that at point C increases. These concentrations then remain almost unchanged until 40 h. Therefore, during the first 20 h of growth, the concentration of carbon impurity at the bottom of the polysilicon ingot tends to decrease with increasing time. Figure 8(b) shows the variation in the carbon impurity concentration in the quartz crucible as a function of growth time and position. The carbon impurity concentration at point A\* decreases from  $2.40 \times 10^{-7}$  kmol/m<sup>3</sup> at 5 h to  $2.37 \times 10^{-7}$  kmol/m<sup>3</sup> at 40 h. Similarly, the carbon impurity concentration at point B\* decreases from  $2.44 \times 10^{-7}$  kmol/m<sup>3</sup> at 5 h to  $2.43 \times 10^{-7}$  kmol/m<sup>3</sup> at 40 h. Conversely, the carbon impurity concentration at point C\* increases from  $2.48 \times 10^{-7}$  kmol/m<sup>3</sup> at 5 h to  $2.53 \times 10^{-7}$  kmol/m<sup>3</sup> at 40 h. These results indicate that the carbon impurity tends to aggregate at the top of the polysilicon ingot, which confirms the efficacy of the directional solidification method for removing the carbon impurity.

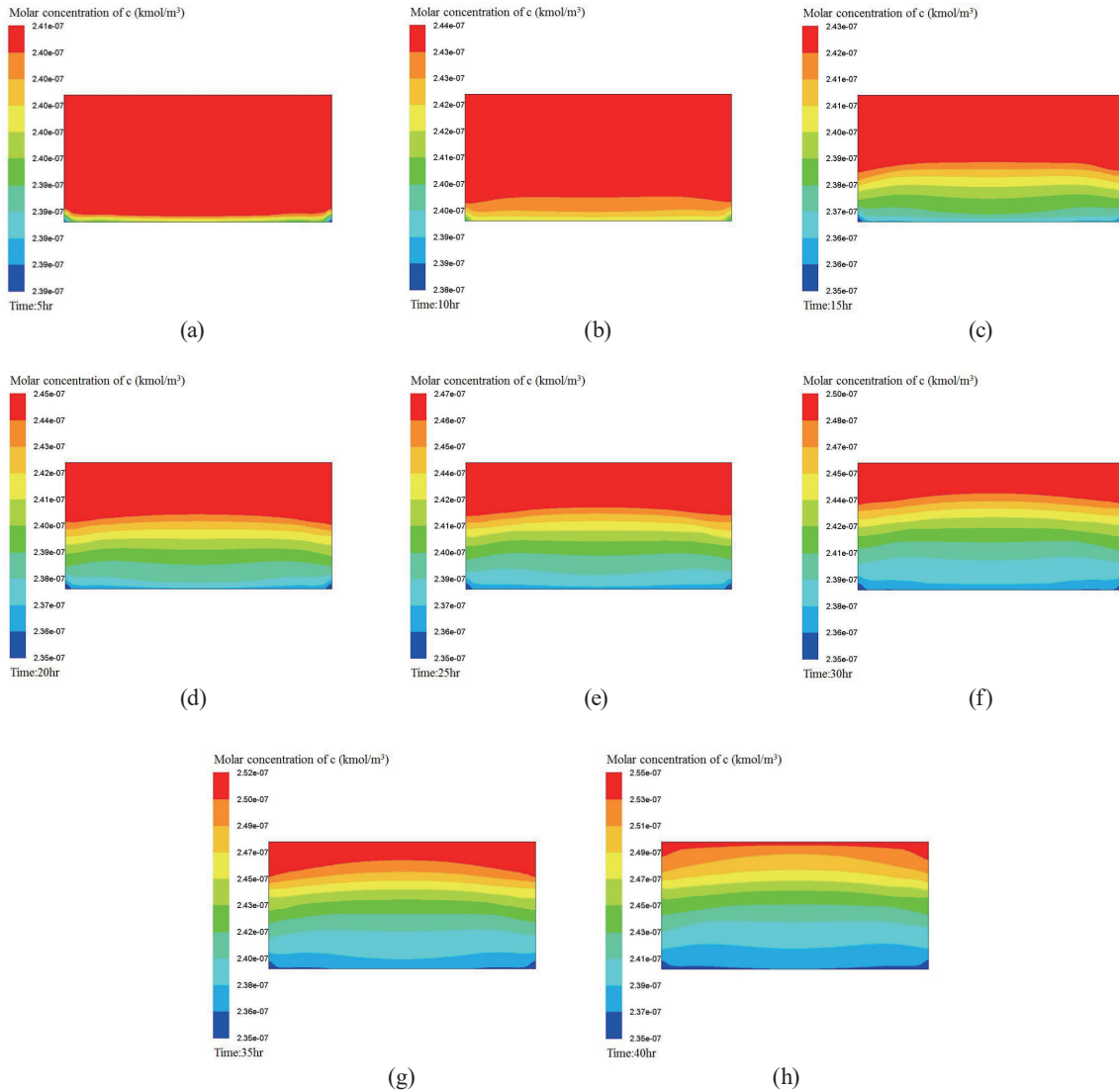


Fig. 7. (Color online) Distribution of carbon concentration in the solid–liquid phase after (a) 5, (b) 10, (c) 15, (d) 20, (e) 25, (f) 30, (g) 35, and (h) 40 h.

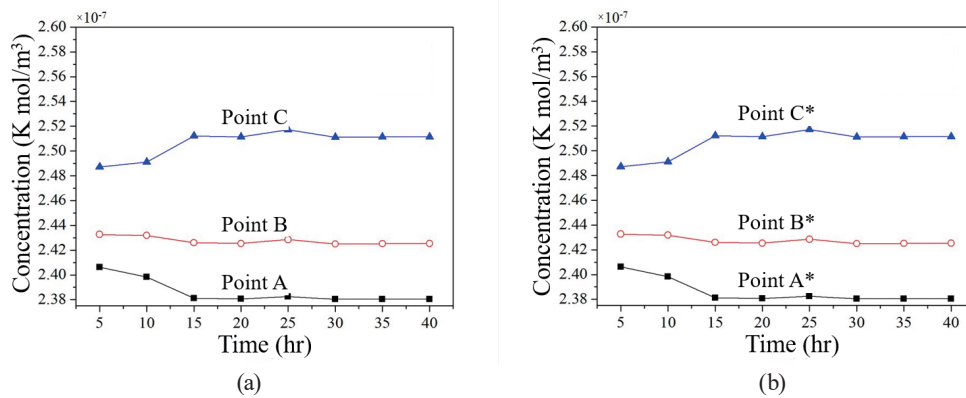


Fig. 8. (Color online) Distributions of carbon concentration in (a) central area and (b) quartz crucible area.

## 4. Conclusions

In this study, the simulation results revealed that the cooling rate in the central area of the furnace was consistently higher than that at the crucible edge. At the beginning of the process, both the CO and oxygen concentrations in the furnace were found to be unevenly distributed. However, increasing the pumping capacity of the argon outlet was found to reduce the concentration of the CO impurity and thereby minimize its diffusion into the polysilicon ingot. The oxygen concentration in the central area slowly moved upward through the segregation effect, resulting in the oxygen concentrating at the top of the polysilicon ingot. Our simulation results clearly demonstrate that during the initial growth stage of the ingot, a higher argon gas flow rate at the inlet can be used to remove impurities. However, in the later stages of growth, a lower argon gas flow rate at the inlet can achieve a more uniform temperature distribution throughout the ingot, thus improving its quality. In addition, the extraction capacity of the gas outlet should be increased over time while lowering the insulation cage, which enlarges the gap at the bottom of the furnace. This facilitates the expulsion of impurities in the direction of the gas flow, ultimately reducing the impurity concentration in the gas phase inside the crystal growth furnace. This study primarily utilizes simulation methods to analyze the process of directional solidification for growing polycrystalline silicon ingots. This approach enables us to understand the concentration variations of impurities within the crystal growth furnace and provides analytical data to further enhance the quality of polycrystalline silicon wafers and achieve higher conversion efficiency.

## Acknowledgments

This work was supported by projects under Nos. MOST 110-2622-E-390-002 and MOST 110-2221-E-390-020, and Xiamen University Tan Kah Kee College Pre-research project YY2019L03.

## References

- 1 M. P. Bellmann, D. Lindholm, and M. MHamdi: *J. Cryst. Growth* **399** (2014) 33.
- 2 J. Dai, Y. C. Yang, C. M. Hsu, H. W. Tseng, P. Wang, and C. F. Yang: *Sens. Mater.* **33** (2021) 2577.
- 3 W. V. Ammon, A. Sattler, and G. Kissinger: *Electronic and Photonic Materials*, S. Kasap and P. Capper Eds. (Springer International Publishing, Switzerland, 2017) 2nd ed., Chap. 5.
- 4 X. Li, Y. C. Yang, C. M. Hsu, H. W. Tseng, J. Zhang, and C. F. Yang: *Sens. Mater.* **33** (2021) 2607.
- 5 L. J. Geerligs, P. Manshanden, G. P. Wyers, E. J. Øvrelid, O. S. Raanes, A. N. Wærnes, and B. Wiersma: *Proc.20th EUPVSEC* (2005) 6–10.
- 6 T. Buonassisi, A. A. Istratov, M. A. Marcus, B. Lai, Z. Cai, S. M. Heald, and E. R. Weber: *Nat. Mater.* **4** (2005) 676.
- 7 S. Binetti, J. Libal, M. Acciarri, M. D. Sabatino, H. Nordmark, and E. J. Øvrelid: *Mater. Sci. Eng. B* **159–160** (2009) 274.
- 8 R. Kvande, Ø. Mjøs, and B. Rynningen: *Mater. Sci. Eng. A* **413–414** (2005) 545.
- 9 L. Liu, S. Nakano, and K. Kakimoto: *J. Cryst. Growth* **310** (2008) 2192.
- 10 L. Raabe, O. Pätzold, I. Kupka, J. Ehrig, S. Würzner, and M. Stelter: *J. Cryst. Growth* **318** (2011) 234.
- 11 A. Lawrenz, M. Ghosh, K. Kremmer, V. Klemm, A. Muller, and H.J. Moller: *Solid State Phenom.* **95–96** (2004) 501.
- 12 G. Du, N. Chen, and P. Rossetto: *Sol. Energy Mater. Sol. Cells* **92** (2008) 1059.
- 13 O. Breitenstein, J. P. Rakotoniaina, M. H. Al Rifai, and M. Werner: *Prog. Photovolt.* **12** (2004) 529.

- 14 D. Vizman, J. Friedrich, and G. Mueller: *J. Cryst. Growth* **303** (2007) 231.
- 15 Y. Delannoy, F. Barvinschi, and T. Duffar: *J. Cryst. Growth* **303** (2007) 170.
- 16 N. Dropka, W. Miller, R. Menzel, and U. Rehse: *J. Cryst. Growth* **312** (2010) 1407.
- 17 Rising Gas: <http://www.risinggas.com/product/1/2010/0310/1.html> (accessed August 2022).